Journal of Civil Structural Health Monitoring (2023) 13:649–659
https://doi.org/10.1007/s13349-023-00671-y

ORIGINAL PAPER

Local defect detection using structural health monitoring with semi-non-contact and fully automated instrumentation

Sikandar Sajid[1,2] · **Luc Chouinard**[2]

Received: 25 October 2022 / Accepted: 3 January 2023 / Published online: 12 January 2023

Abstract
An efficient and fully automated global health monitoring approach to detect and quantify local defects in reinforced concrete slabs with minimal equipment and without the need of baseline information is proposed as an alternative to presently used non-destructive test (NDT) methods. Such defects are generally detected locally through a sequence of measurements over a grid at the surface of an element with stress-wave or electromagnetic-based NDT. It is shown that the delineation of local defects can also be obtained by using structural health methodologies, on high-frequency measurements, similar to those from stress-wave NDT methods but with higher efficiency. In this application, data are obtained by using an automated roving laser vibrometer and an automated modal impactor with load cell, eliminating the need to physically move the impactor and sensor over each location of the grid. Experimental measurements were performed on a reinforced concrete slab with built-in defects consisting of delaminations at different depths, debonding, and honeycomb. The location of the automated impactor is kept at a fixed position while the laser beam measurements are performed sequentially at a grid of locations on the surface of the plate. A comparison of the frequency response functions (FRFs) at each point indicates that for resonant peaks above 700 Hz, higher responses are obtained at locations above defects. The spatial contour plots of the FRFs at respective resonant frequencies (i.e. 796 Hz, 1327 Hz, and 1854 Hz) are shown to correspond to the locations of the debonding, shallow delamination, and deep delamination. The defect detection and delineation is compared to results obtained from the C-scan generated with ultrasonic shear-wave tomography, and from impulse-response test data analyzed with a recently proposed statistical pattern recognition procedure. The detection and localization of the local defects with the more efficient automated health monitoring approach is shown to be comparable to those obtained with the two selected local NDT methods. The proposed approach provides a viable process to implement quality control in prefabricated concrete elements that are not currently in-practice.

Keywords Structural health monitoring · Nondestructive test · Delamination · Impulse-response test · Concrete slab · Ultrasonic shear-wave tomography

1 Introduction

Condition assessment of civil structures is performed to assess material and/or structural integrity. Structural integrity methods are based on the global response of the structure [1] using, for example, operational modal analysis or experimental modal analysis in comparison to baseline information from the initial state of the structure. These assessment methods are typically not affected by localized defects since they are obtained using low-frequency vibration measurements [2, 3]. Localized defects such as honeycomb, delamination, debonding, voids, etc. are assessed using non-destructive test (NDT) methods, which generally use the response from controlled or measured excitation as the basis for defect detection and characterization. NDT methods are performed at relatively higher frequencies in comparison to structural health monitoring (SHM) methods and provide more detailed and localized assessments but require more time to complete [4]. A survey of NDT

✉ Luc Chouinard
luc.chouinard@mcgill.ca

Sikandar Sajid
sikandar.sajid@mail.mcgill.ca

[1] Civil Engineering, McGill University, Montreal, Canada

[2] Civil Engineering, University of Engineering & Technology, Peshawar, Pakistan

methods used in practice for the condition assessment of concrete in structures is provided in the consensus committee report of ACI 228.2R13 [5]. Among these, the most versatile tests are the impact-echo [6], impulse-response [7, 8], ground penetrating radar [9], infrared thermography [10], and ultrasonic shear-wave tomography tests [11]. The impact-echo works on the basis of propagation and reflection of P-waves due to changes in the acoustic impedance owing to anomalies, boundary layer of the test element and reinforcing steel. It has a well-established theoretical basis and is used for defect detection and characterization. However, the test takes a long time to complete, which limits its application to the investigation of defects at locations that have been previously identified with other test methods. Air coupled sensors have been introduced to replace contact sensors to reduce the time needed for performing measurements [12, 13]. However, tuning of the impactor to the desired frequency range can be time-consuming and remains an impediment. The impulse-response test (IRT) is a low-strain and low-frequency stress-wave method, which uses standing waves and the relative variation of dynamic responses across the test element as the basis of detection. The test method is widely used as a fast scanning NDT method for which the theoretical basis has recently been reported [14]. Recently, new signal processing techniques based on statistical pattern recognition and clustering together with homoscedasticity [15, 16] have been proposed to improve damage detection. However, detectability is mostly limited to shallow defects (< 250 mm) [14]. Ground penetrating radar (GPR) can also be used to scan large surfaces. It is based on the propagation of electromagnetic waves and their reflection due to differences in electrical impedance from defects, metallic elements, and the boundary of the test element. However, GPR has limitations due to the interpretability of test results [17–20] and detectability of defects below reinforcing steel can be challenging. Infrared thermography is a fast and efficient non-contact NDT method for shallow defect detection [21]. However, this method has robustness issues due to variations in the exposure conditions [10]. The ultrasonic shear-wave tomography is used to generate 3D tomograms of objects using a synthetic aperture focusing technique (SAFT) [22]. The method is highly accurate and is routinely used to assess the integrity of pre-stress tendon grouts [23]. The main limitation of this test is the relatively long time needed to perform the test.

The use of the global methods for defect detection in concrete structures is widely reported in the literature [24]. In most instances, a comparison of the generated dynamic parameters with baseline information is used to make inferences on the detection and localization of the defects [2]. Xing et al. [25] report detecting delamination of different sizes in concrete plates using resonant frequency shifts in comparison to undamaged specimens. This technique is shown to be performing reasonably well; however, the shifts in the resonant frequencies can also be partly due to changes in the environmental conditions, which can induce uncertainties in detection. The detection and localization of local defects in a bridge deck have also been obtained by using experimental modal analysis and identifying local decreases in stiffness by comparison to baseline data [26]. Similarly, damage sensitive indicators based on measured modal parameters obtained using the global methods to detect local fatigue damages have been used but require prior knowledge or baseline information of the test structure [27]. The current state-of-the-art also report local damage detection using global methods with some damage sensitive features but without the need for prior information on the condition of the test structures. Ratcliffe [28] reported detection and localization of saw cut cracks in a cantilever steel beam and used experimental modal analysis on a closely spaced grid to generate displacement frequency response functions. These are then converted to curvature functions to yield a damage sensitive feature, which efficiently detect small defects without requiring baseline information. However, this was applied to a one-dimensional beam and experimental modal analysis measurements using a roving hammer and stationary sensor on a 25.4 mm square grid, which limits the application of the proposed procedure to small test elements. The frequency range used in their experiments was 0–1560 Hz and the resonant frequencies were not being able to delineate smaller defects [28]. This method was also applied to a composite bridge deck to detect local defects and manufacturing anomalies but the inferences on the presence of defects can be time consuming due to placement of sensors on a fine grid [29]. Furthermore, the application for the data analysis of this procedure is simpler for the 1D structures such as in [28] but relatively more complicated, especially the interpretation of the results, for a 2D structure such as bridge deck [29]. More recently, a fully non-contact high-frequency global method using Rayleigh waves was used to detect and localize delamination in concrete [30]. A single axis laser Doppler vibrometer is used for measurements and a laser-induced plasma shock wave provides the impact on the specimen. The delamination was detected; however, the approach requires that the impact is applied both at defect and no-defect solid locations implying that the location of the defect would be needed as a prior information or use a fine grid pattern of measurements in which case, it is expected to be time consuming from the instrumentation adjustment perspective given that the shock-wave has to be applied at each point.

The objective of this research is to propose and demonstrate a local damage detection method based on a global structural health monitoring approach using high-frequency response data and automated instrumentation that does not require any baseline information. Such defects are generally

detected with locally applied NDT methods that have relatively low efficiency and inherent limitations. The diagnostics of the proposed method applied to an experimental reinforced concrete slab with simulated defects are compared to those from two commonly used local NDT methods, the impulse-response test and the ultrasonic shear-wave tomography.

The article is organized by first providing the description of the experimentation and measurement scheme of the global method with the proposed instrumentation. Next, the detection results are provided for the global test method with the proposed instrumentation along with the technical details for performing the test. This is followed by a comparison of the performance of the proposed detection procedure with those of two local NDT methods, the impulse-response, and the ultrasonic shear-wave tomography. The article is concluded by providing a discussion on the results of both the global and the local methods used.

2 Condition assessment with global method

2.1 Test specimen

The experimental slab is 300 mm in thickness with planar dimensions of 1200 mm by 2400 mm and is resting on a flat uniform surface provided by a plywood sheet that is fully supported on a smooth concrete floor. The edges of the slab are not restrained. It is reinforced with 15 M Grade 60 steel bars in both directions at 200 mm spacing on the bottom and top of the slab. Defects simulating delamination (at two different depths), honeycomb, debonding, and pipes partially filled with grout are built in the experimental slab (Fig. 1). The delaminations are simulated by using 25 mm thick circular polystyrene foam boards having diameters of 400 mm. The shallow and deep delaminations are located at depths of 80 mm and 220 mm, respectively (Fig. 1b). Debonding is simulated by placing a thin glass fiber sheet at a depth of 40 mm from the top surface. The honeycomb is simulated using a 140 mm thick precast concrete block having planar dimensions of 350 mm by 400 mm and constructed using a small quantity of fine aggregates so that voids exist between coarse aggregate particles. The pipes simulate prestressing tendon ducts, one of which is filled with grout and the other is empty.

The slabs are constructed with the Ministry of Transportation of Quebec Type 5 concrete mixture having a compressive strength of 35 MPa, which is typically used in pavements and bridge decks in Quebec, Canada.

2.2 Instrumentation and measurements

The instruments included a PSV QTec® (S/N 336814) multi-point laser vibrometer for automated response time history measurement in velocity domain and a Wavehit® automated hammer (Fig. 2). The Wavehit® hammer is a Scalable Automatic Modal (SAM) Hammer (Fig. 3) with a load cell and a scalable usable frequency range induced by the hammer in each measurement. The measurements are performed in an experimental modal analysis setup, keeping the modal hammer at the same location and roving sensing across the surface of the slab with the laser beam to measure the vibrations. The PSV QTec® laser vibrometer can perform measurement automatically and

(a)

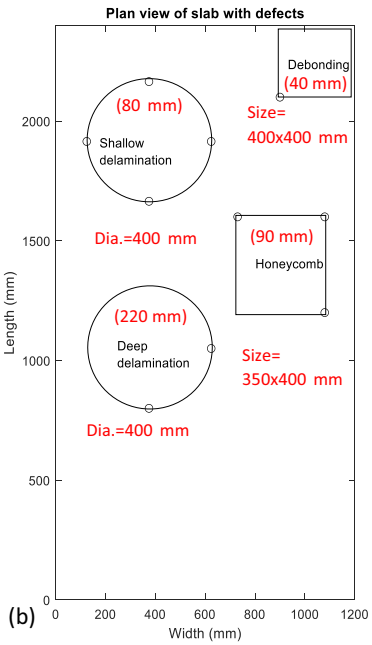

(b)

Fig. 1 (**a**) Experimental slab, and (**b**) the plan view showing simulated defects with the depth values given in parenthesis inside each defect

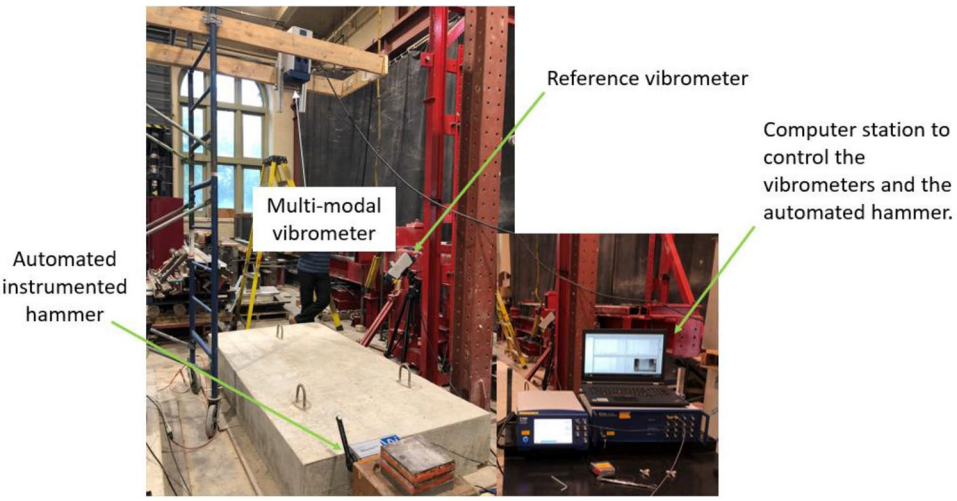

Fig. 2 Test setup showing instrumentation and their installation

Fig. 3 Scalable automatic modal (SAM) hammer by Wavehit®

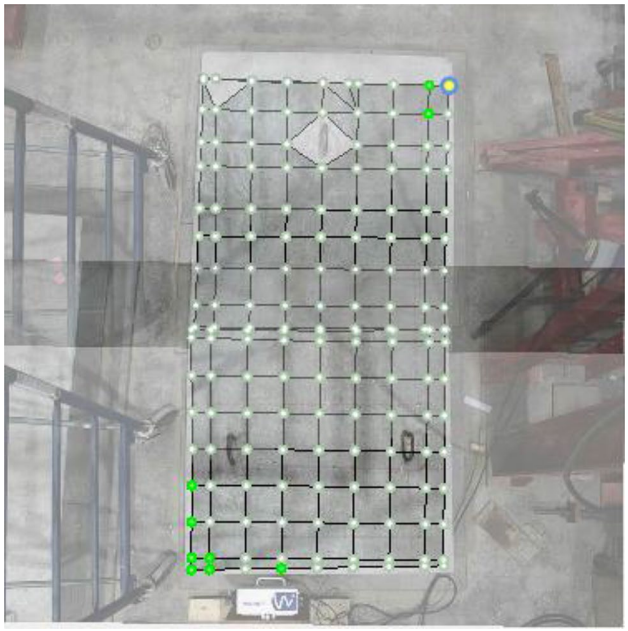

Fig. 4 Grid of measurement points for the two stitched virtual frames

sequentially on a pre-defined grid with a single input and single output (SISO) setup. The vibrometer is installed above the test specimen such that the entire specimen is visible in a single camera frame by locating it at a height above the specimen equal to or greater than the longest dimension of the specimen. In the current application, the vibrometer was installed at a nominal height of 2000 mm above the slab, which is less than its longer dimension of 2400 mm (Fig. 2). Therefore, the measurements were performed using two separate virtual frames that were subsequently stitched to generate deflection shapes (Fig. 4).

2.3 Data analysis and results

After defining the grid points and performing the measurements, the FRFs are calculated for each of the test points. The data analysis and defect delineation procedure is outlined in Fig. 5. Next, the average FRF for all test points is calculated as shown highlighted in Fig. 6. It can be noticed that some FRFs are distinctively higher at resonant frequencies upwards of 700 Hz, which is treated as the upper range of frequencies in contrast to the frequency range below 700 Hz in which the peaks are more "compact" and do not show any distinct FRF values (Fig. 6). The peaks in the lower frequency range (i.e., less than 700 Hz) are associated

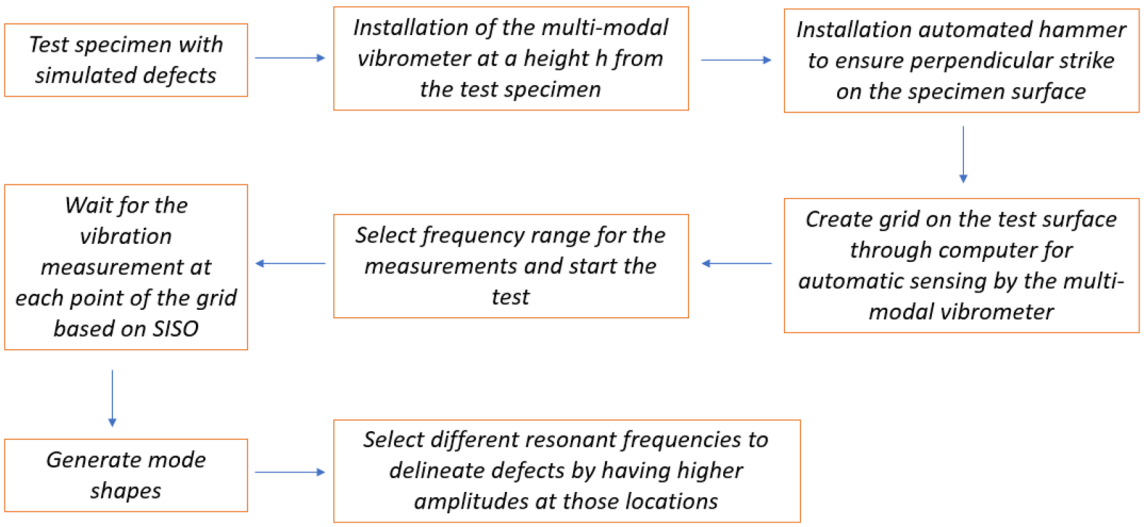

Fig. 5 Flowchart of measurements and data analysis

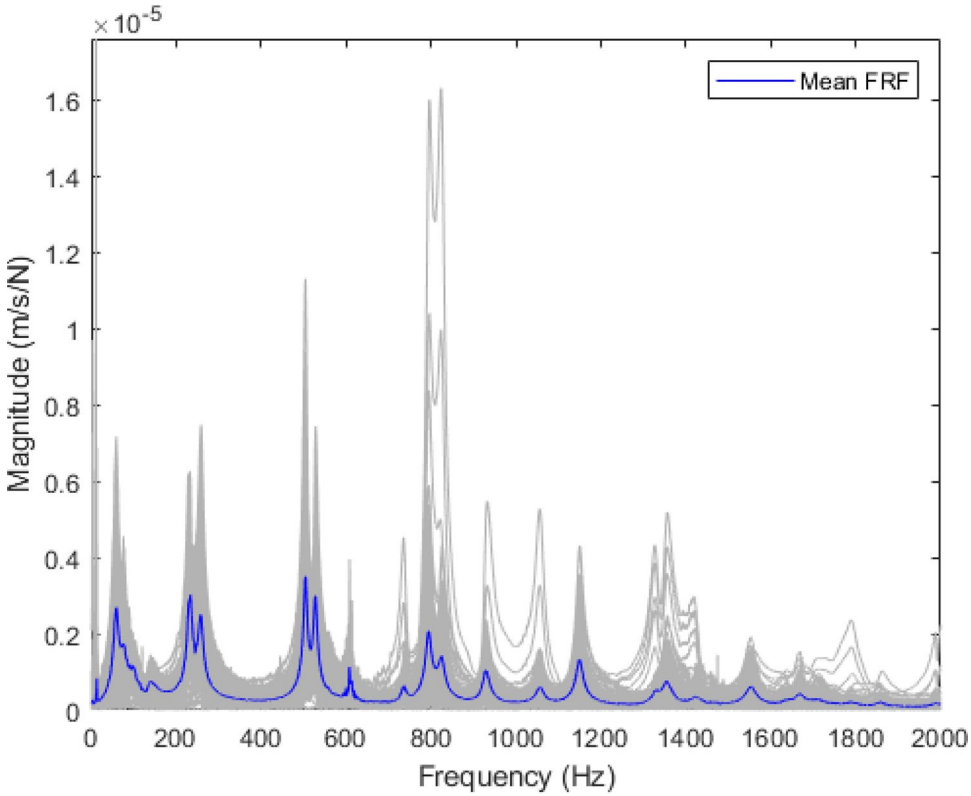

Fig. 6 FRFs at all the test points with highlight mean FRF

with the dominant modes for the entire plate while the peaks in the upper range can be associated with the effects of local defects and can easily be distinguished in the contour plots of the FRF values at selected resonant frequencies (Fig. 7).

Figure 7 shows the contour plot of the FRF values at three selected resonant frequencies in the upper frequency range for all the measurement locations. The first contour plot of the FRF values at 796 Hz shows a uniform response except at a location above the debonding defect (Fig. 7a). A test point at the top left corner was removed as an outlier due to out-of-range deformations. Similarly, at 1327.5 Hz, the FRF values obtained show disproportionally high trend in the portion of the slab above the shallow delamination compared to the rest of measurement locations as demonstrated

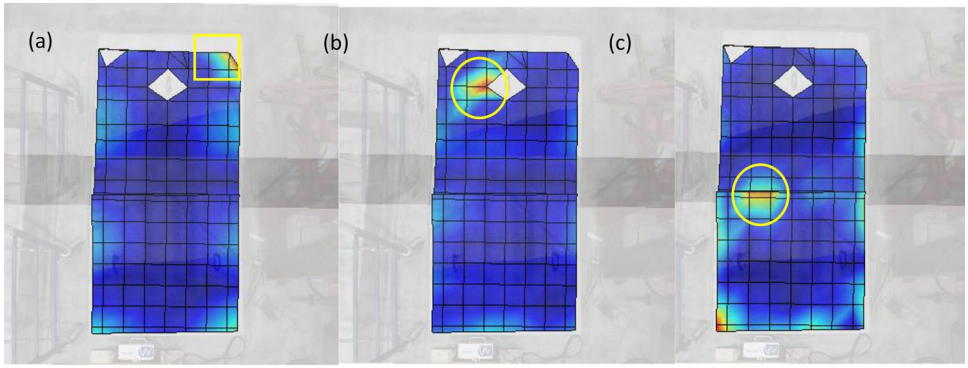

Fig. 7 Mode shapes delineating (**a**) debonding at 796 Hz, (**b**) shallow delamination at 1327.5 Hz, and (**c**) deep delamination at 1854.5 Hz

in Fig. 7b. Furthermore, at 1854.5 Hz, similar high deformation can be observed above the deep delamination (Fig. 7c). The deformation of the plate above the deep delamination at 1854.5 Hz is around one order of magnitude lesser than that on the shallow delamination at 1327.5 Hz. Large deformations are also observed in the lower corner of the specimen at 1854.5 Hz and is possibly attributable to the proximity of the test point to the corner edge of the specimen. Using the contour plot of the FRF values at the afore-mentioned resonant frequencies, the debonding, shallow and deep delaminations are accurately delineated. The honeycomb portion is not detectable within the frequency range under study (0 to 2000 Hz) and will be further investigated by using a higher frequency range as well as by comparison with baseline information.

2.4 Technical considerations for practical applications

In the preceding sections, the experimental modal analysis with roving sensor is shown to efficiently delineate delamination type defects. Similar testing procedures are ubiquitous for quality control in the automotive and aerospace industry but are not currently used for structural assessments of the infrastructure. In the latter case, operational modal analysis (OMA) using ambient noise has been favored given the large masses of typical structures. OMA is used to characterize the dynamic properties of the structure, which can be compared to baseline information from previous health monitoring surveys. For experimental modal analysis (EMA), the modal hammer used in testing must be selected to excite a frequency range that includes the resonant frequencies of the plate above the defects (delaminations and debonding). The modal hammer must also be adequate to engage the global responses of the specimen considering the damping of the system. The interdependencies between the frequency range and energy of the hammer and the damping of the system are qualitatively illustrated in Fig. 8. For example, the dashed rectangle outlines qualitatively the range of hammer properties that would be appropriate for performing condition surveys on civil engineering structural members having reinforced concrete as base material by having enough energy transmitted to generate global response while also keeping the frequency high enough to excite local modes. A more detailed discussion on the selection of excitation frequencies and the energy transmitted by modal hammers can be found in [31, 32]. The global method proposed here can be sensitive to the local defects and hence can be implemented in the prefabricated concrete industry for the quality control of the finished products. The ease and lesser time for the completion of the measurements can be a viable quantitative procedure for the detection and localization of defects and material level post production quality assurance of the prefabricated concrete elements. A detail description of the implementation of the proposed procedure for the precast members requires a separate study and is beyond the scope of this article.

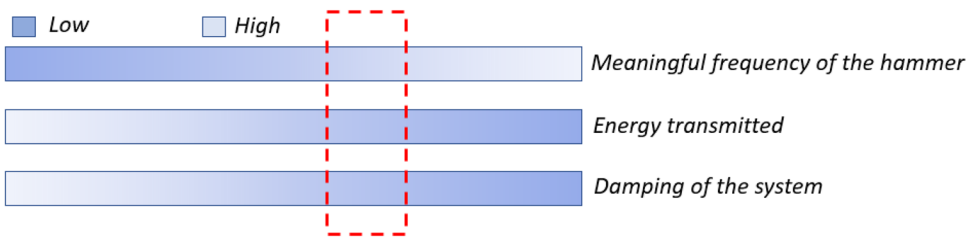

Fig. 8 Qualitative relationship of the important parameters in the proposed global assessment procedure for local defect detection

3 Condition assessment with local NDT methods

The condition assessment of the plate is also performed with the impulse-response test and ultrasonic shear-wave tomography in order to compare the performance of the proposed global assessment procedure to local NDT assessments.

3.1 Impulse-response test

The impulse-response test [7] is a low-strain and low-frequency stress-wave based NDT method, which is widely used to assess large surfaces as a fast scanning method [33]. Originally developed for the integrity testing of the drilled shaft piles in Europe in 1960's, the NDT community developed several applications of this method since 1980's for the condition assessment of test structures other than drilled shaft piles. These included condition assessment of bridge decks [34], floor slabs [35], concrete chimneys [36], highway pavements [37], concrete tunnel linings [38], radioactive waste tanks [39], reinforced concrete pedestals for antenna [40], and nuclear containment buildings [41]. Sajid and Chouinard provide a detailed literature review and current state-of-the-art of the test [8].

The standard practice for the test is described in ASTM C1740 [7]. First, a square grid of the desired size is marked on the test element and impulse and response measurements are recorded using both the sensor and hammer roving simultaneously and sequentially on the grid points to finally generate velocity frequency response functions at each measurement location on the marked grid. Several indices within 10–800 Hz capturing the shape features of the generated velocity FRF or mobility spectra are calculated in different frequency ranges. The relative variation of these indices is used empirically as the basis of detection with the test. More recently, the physical basis of the test is presented by Sajid et al. [14] showing that the standing waves and the relative variation of the dynamic characteristics form the basis of detection with the test. The currently used damage indices are the average mobility (M_{av}), dynamic stiffness (K_d), voids index (v), and mobility slope (M_s) which are defined and illustrated in Fig. 9 and the mobility is defined as the peak velocity per unit impact force at a specific frequency for a concrete plate element with a description of the indices according to ASTM C1740 [8].

Impulse-response test measurements were performed on the RC slab with simulated defects using a PCB 352C33 piezoelectric accelerometer, an PCB 086D05 modal hammer, and National Instrument NI-6123 USB card for data acquisition with signal conditioner. The impulse-response measurements were recorded at a sampling frequency of 10 kHz (for a duration of 0.4096 s) according to the protocols of ASTM C1740 on a square grid of 300 mm by 300 mm and the accelerance spectrum generated of each test point is obtained using Eq. 1 in which $a(t)$ and $f(t)$ are, respectively, the response and force time histories obtained for each measurement, and FFT represents the fast Fourier transform.

$$Accelerance = \left| \frac{FFT(a(t))}{FFT(f(t))} \right|. \tag{1}$$

In practice, the average mobility is used for the diagnostics of the test element as recommended by several authors [40, 42, 43]. Sajid et al. [15] proposed an unsupervised

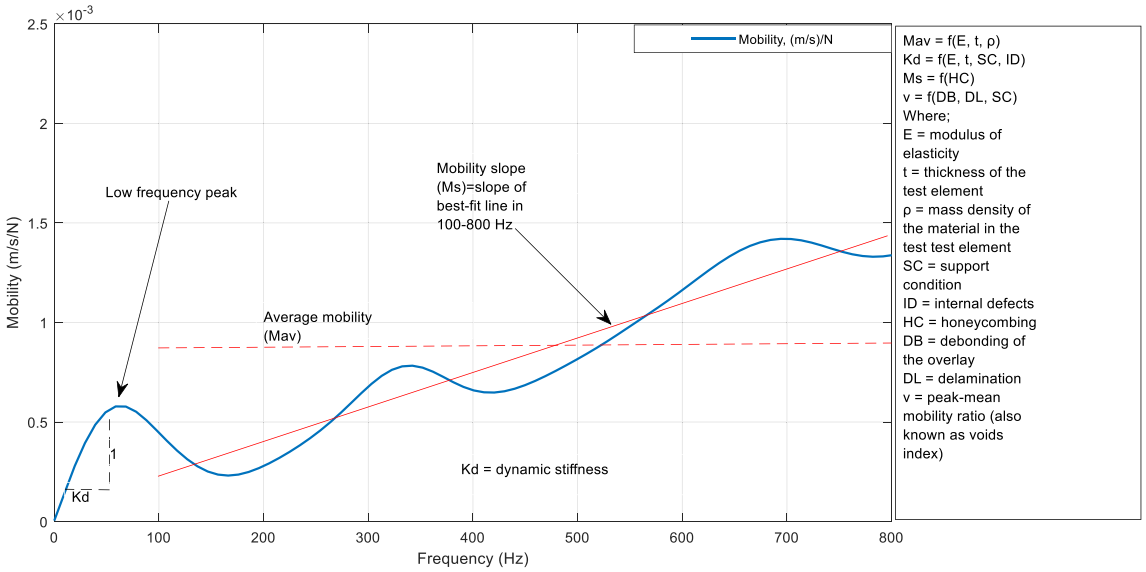

Fig. 9 A typical velocity frequency response function generated with impulse-response

approach based on affinity propagation and homoscedasticity and manifest better accuracy compared to the average mobility. However, a recently proposed data analysis technique based on statistical pattern recognition, which have been shown to outperform the diagnostics based on the average mobility, is used in this instance [16].

Consider a set of FRFs (the feature matrix) from impulse-response test measurements composed of m test points and n frequencies arranged in a matrix A of m rows and n columns,

$$[A] = \begin{bmatrix} A_{1,1} & \cdots & A_{1,n} \\ \vdots & \ddots & \vdots \\ A_{m,1} & \cdots & A_{m,n} \end{bmatrix}. \quad (2)$$

The element A_{ij} represents the FRF value at the jth frequency for ith test point on a test element. Principal component analysis on the covariance of the matrix in Eq. 2 is used to obtain dominant patterns in calculating factor scores based on the first few principal components. The box and whisker plot is used to identify the extreme outliers in the factor score values for each principal component. After the impulse-response measurements are performed on the grid shown in Fig. 10a, the FRFs are combined in a feature matrix in a frequency range of 10–1200 Hz. Principal component analysis on the covariance matrix is performed showing that the first 3–4 principal components explain most of the variability in the feature matrix as shown by the scree plot in Fig. 10c. The box whisker plot is obtained for factor scores based on the first three principal components show that the extreme outliers are present only in the factor scores for the first and second principal components (Fig. 10d). Therefore, the contour plots of the factor scores based on the respective principal components is calculated as shown in Fig. 10e, f. It can be noticed that the debonding and shallow delamination are delineated by the factor scores based on the first principal component (Fig. 10e), while the deep delamination and the honeycomb are detected by the factor score for the second principal component.

3.2 Ultrasonic shear-wave tomography

Ultrasonic shear-wave tomography is used to generate 3D tomograms of objects using a synthetic aperture focusing technique (SAFT) [22]. It uses the reflection of shear-wave

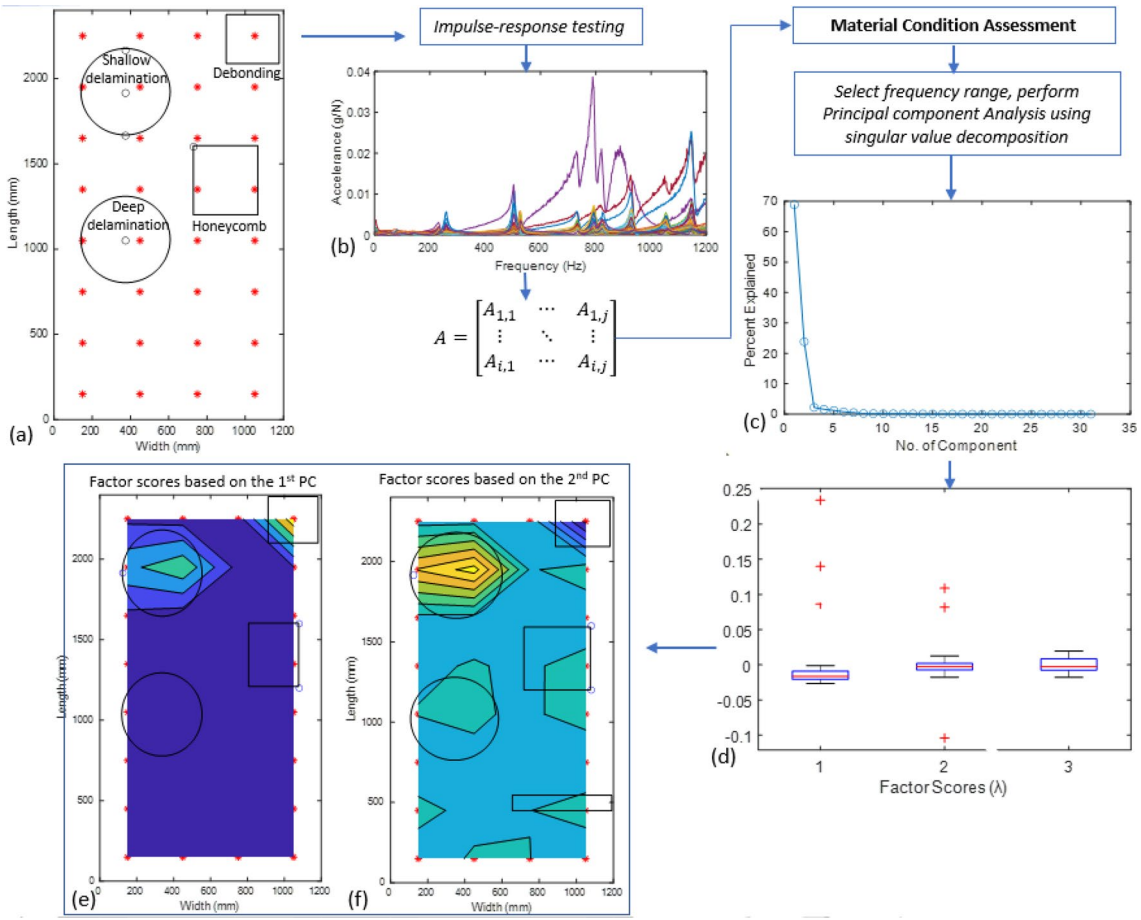

Fig. 10 Defect detection in reinforced concrete slab using statistical pattern recognition procedure

due to the changes in material impedance as the basis of detection. The method is highly accurate and is routinely used to assess the integrity of grouted tendon ducts in post-tensioned members [23]. The main limitation of this method is the relatively longer time required to gather data from a large structure. In this research, PUNDIT PL200 by Proceq Inc. is used to generate C-Scan. For this purpose, a grid of 10 by 22 with each grid size of 100 mm is used on the test reinforced concrete slab to perform the measurements (Fig. 11). Smooth surfaces are generally needed to ensure proper contact and correct record of the sensors in the PUNDIT PL200. The C-scan generated this way is shown in Fig. 12. It can be seen that the deep delamination and the honeycomb are efficiently delineated. The shallow delamination is also delineated but not as accurately as the deeper one. The debonding is not readily detected with the selected resolution of the shear-wave velocities. The grout infill, which is generally detected by ultrasonic shear-wave tomography is detected to a limited extent.

4 Concluding remarks

This research combines the higher efficiency of the global health monitoring approaches with automated instrumentation and the relatively higher frequency of the local-based NDT methods to demonstrate a defect detection approach which can efficiently and accurately perform diagnostics of the concrete slabs. The main contribution of the article is the demonstration that automated instrumentation in a global health monitoring framework can detect local defects in a reinforced concrete slab without requiring baseline information and/or the knowledge of the location of the defects. The second important contribution is the validation of the procedure by comparing defect delineation obtained with the

Fig. 11 Ultrasonic shear-wave tomography measurement on a grid of 10 by 22 points with the grid size as 100 mm using PUNDIT PL200

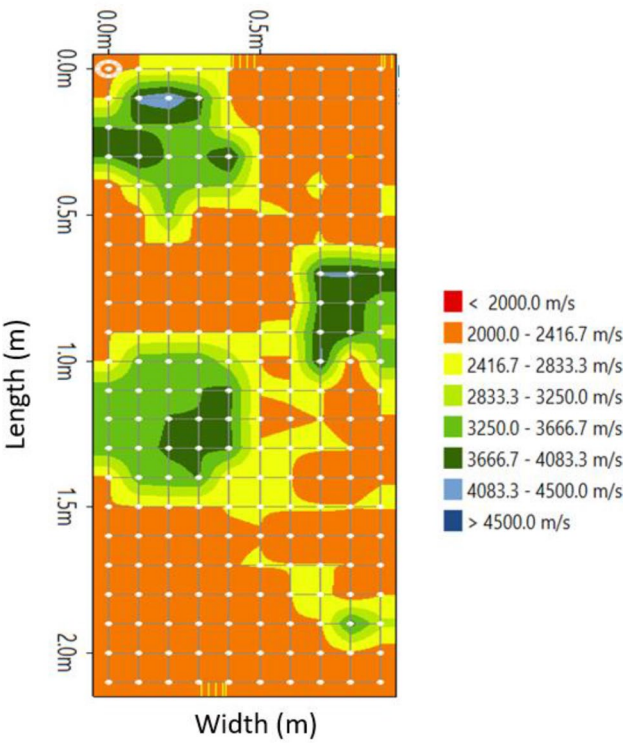

Fig. 12 C-Scan of the test slab generated with the ultrasonic shear-wave tomography

global health monitoring approach with the condition assessment using two widely used local-based NDT methods.

In this research, automated instrumentation-driven experimental modal analysis with high-frequency range is shown to excite fundamental modes of the portion of the plates above a defect. A fully supported reinforced concrete slab having unrestrained edges and simulated delamination at different depths, debonding, and honeycomb is used for experimentation. It is demonstrated that the FRF values at the selected resonant frequencies were distinctly higher in some cases in the frequency ranges beyond 700 Hz. The contour plots of the FRF values at these selected resonant frequencies, which are 796 Hz, 1327 Hz, and 1854 Hz, for all the measurement locations, respectively, delineated the debonding, shallow delamination, and deep delamination. The detection is performed without the need of baseline information and with much higher efficiency due to the use of fully auomated instrumentation. The diagnostics of the proposed approach are compared with two widely used stress-wave local-based NDT methods; the impulse-response test and the ultrasonic shear-wave tomography. The ultrasonic shear-wave tomography is demonstrated to delineate the delamination at both the depths, and the honeycomb. However, the debonding is not fully detected with the ultrasonic shear-wave tomography for the given resoultion of the reflected shear-wave velocities. The impulse-response test is

able to detect the shallow delamination and debonding, but the deeper delamination and honeycomb were observed with limited detectability using the statistical pattern recognition approach for data analysis with the test. Overall, the global assessment is shown to have higher efficiency given automation and with accuracy comparable to the highly refined yet time-consuming ultrasonic shear-wave tomography test and the local-based fast scanning method of impulse-response test.

The authors believe the defect characterization may also be performed with the proposed procedure, however, furture work involving higher number of data points and experimentally validated numerical simulations is recommended to make meaningful inferences on that aspect of the global health monitoring approach for local defect detection.

Acknowledgements The authors appreciate Mario Pineda and David Damiani from Polytec Inc. for lending the instrumentation used for the global assessment in this research and assistance in the measurements on the experimental specimen constructed by the authors of this study. The assistance in the ultrasonic shear-wave tomography measurements by Farah Artin and Thomas Yin, McGill University, Civil Engineering undergraduate students as part of their summer undergraduate research project is acknowledged. The authors appreciate the Natural Science and Engineering Research Council (NSERC) Discovery grant to fund this research.

Data availability Data for this research may be shared upon reasonable request and approval from the people and/or organization(s) involved in this research.

Declarations

Conflict of interest The authors declare no conflict interest.

References

1. Farrar CR, Worden K (1851) An introduction to structural health monitoring. Philos Trans R Soc A Math Phys Eng Sci 2007(365):303–315
2. Worden K, Farrar CR, Manson G, Park G (2007) The fundamental axioms of structural health monitoring. Proc R Soc A Math Phys Eng Sci 463(2082):1639–1664
3. Farrar CR, Doebling SW, Nix DA (2001) Vibration–based structural damage identification. Philos Trans R Soc Lond Ser A 359(1778):131–149
4. Chen JG, Davis A, Wadhwa N, Durand F, Freeman WT, Büyüköztürk O (2017) Video camera–based vibration measurement for civil infrastructure applications. J Infrastruct Syst 23(3):B4016013
5. ACI-Committee-228 (2013) Nondestructive test methods for evaluation of concrete in structure. *Report ACI 228.2R*. Farmington Hills
6. ASTM-C1383–15 (2015) Standard test method for measuring the p-wave speed and the thickness of concrete plates using the impact-echo method. ASTM International, West Conshohocken, PA, 2015, www.astm.org
7. ASTM-C1740–16 (2016) Standard practice for evaluating the condition of concrete plates using the impulse-response method. ASTM International, West Conshohocken, PA, 2016, www.astm.org
8. Sajid S, Chouinard L (2019) Impulse response test for condition assessment of concrete: a review. Constr Build Mater 211:317–328
9. ASTM-D6432–11 (2011) Standard guide for using the surface ground penetrating radar method for subsurface investigation. ASTM International, West Conshohocken, PA, 2011, www.astm.org
10. Büyüköztürk O (1998) Imaging of concrete structures. NDT E Int 31(4):233–243
11. Choi P, Kim D-H, Lee B-H, Won MC (2016) Application of ultrasonic shear-wave tomography to identify horizontal crack or delamination in concrete pavement and bridge. Constr Build Mater 121:81–91
12. Zhu J, Popovics JS (2007) Imaging concrete structures using air-coupled impact-echo. J Eng Mech 133(6):628–640
13. Ham S, Popovics J (2015) Application of micro-electro-mechanical sensors contactless NDT of concrete structures. Sensors 15(4):9078–9096
14. Sajid S, Chouinard L, Taras A (2022) Developing a new understanding of the impulse response test for defect detection in concrete plates. J Eng Mech 148(1):04021125
15. Sajid S, Chouinard L, Carino N (2022) Condition assessment of concrete plates using impulse-response test with affinity propagation and homoscedasticity. Mech Syst Signal Process 178:109289
16. Sajid S, Taras A, Chouinard L (2021) Defect detection in concrete plates with impulse-response test and statistical pattern recognition. Mech Syst Signal Process 161:107948
17. Sun H, Pashoutani S, Zhu J (2018) Nondestructive evaluation of concrete bridge decks with automated acoustic scanning system and ground penetrating radar. Sensors 18(6):1955
18. Tarussov A, Vandry M, De La Haza A (2013) Condition assessment of concrete structures using a new analysis method: ground-penetrating radar computer-assisted visual interpretation. Constr Build Mater 38:1246–1254
19. Kang M-S, Kim N, Lee JJ, An Y-K (2019) Deep learning-based automated underground cavity detection using three-dimensional ground penetrating radar. Struct Health Monitor
20. Asadi P, Gindy M, Alvarez M (2019) A machine learning based approach for automatic rebar detection and quantification of deterioration in concrete bridge deck ground penetrating radar B-scan images. KSCE J Civ Eng 23(6):2618–2627
21. Clark MR, McCann DM, Forde MC (2003) Application of infrared thermography to the non-destructive testing of concrete and masonry bridges. Ndt E Int 36:4
22. Aldo O, Samokrutov AA, Samokrutov PA (2013) Assessment of concrete structures using the Mira and Eyecon ultrasonic shear wave devices and the SAFT-C image reconstruction technique. Constr Build Mater 38:1276–1291
23. Martin J, Broughton K, Giannopolous A, Hardy M, Forde M (2001) Ultrasonic tomography of grouted duct post-tensioned reinforced concrete bridge beams. NDT E Int 34(2):107–113
24. Sohn H, Farrar CR, Hemez FM, Shunk DD, Stinemates DW, Nadler BR et al (2003) A review of structural health monitoring literature: 1996–2001. Los Alamos National Laboratory, USA, p 1
25. Xing S, Halling MW, Barr PJ (2012) Delamination detection of reinforced concrete decks using modal identification. J Sens
26. Karbhari VM, Kaiser H, Navada R, Ghosh K, Lee L (2005) Methods for detecting defects in composite rehabilitated concrete structures
27. Radzieński M, Krawczuk M, Palacz M (2011) Improvement of damage detection methods based on experimental modal parameters. Mech Syst Signal Process 25(6):2169–2190
28. Ratcliffe CP (2000) A frequency and curvature based experimental method for locating damage in structures. J Vib Acoust 122(3):324–329

29. Crane RM, Gillespie Jr JW, Heider D, Eckel DA, Ratcliffe CP (eds) (2000) Monitoring and defect detection of an all-composite road bridge. ASME International Mechanical Engineering Congress and Exposition. American Society of Mechanical Engineers
30. Wakata S, Hosoya N, Hasegawa N, Nishikino M (2022) Defect detection of concrete in infrastructure based on Rayleigh wave propagation generated by laser-induced plasma shock waves. Int J Mech Sci 218:107039
31. Sajid S, Chouinard L, Carino N (2019) Robustness of resonant frequency test for strength estimation of concrete. Adv Civ Eng Mater 8(1):451–462
32. Carino NJ (2013) Training: often the missing link in using NDT methods. Constr Build Mater 38:1316–1329
33. Davis AG (2003) The nondestructive impulse response test in North America: 1985–2001. NDT E Int 36(4):185–193
34. Davis A, Hertlein B (1990) Assessment of bridge deck repairs by a non-destructive technique. Bridge evaluation, repair and rehabilitation. Springer, Berlin, pp 229–233
35. Davis A, Hertlein B (eds) (1987) Nondestructive testing of concrete pavement slabs and floors with the transient dynamic response method. Proc Int Conf Struct Faults Repair (Lond)
36. Davis AG, Hertlein BH (eds) (1995) Nondestructive testing of concrete chimneys and other structures. Nondestructive evaluation of aging structures and dams. International Society for Optics and Photonics.
37. Davis A, Hertlein B, Lim M, Michols K (eds) (1996) Impact-echo and impulse response stress wave methods: advantages and limitations for the evaluation of highway pavement concrete overlays
38. Davis AG, Lim MK, Petersen CG (2005) Rapid and economical evaluation of concrete tunnel linings with impulse response and impulse radar non-destructive methods. NDT E Int 38(3):181–186
39. Davis AG, Evans JG, Hertlein BH (1997) Nondestructive evaluation of concrete radioactive waste tanks. J Perform Constr Facil 11(4):161–167
40. Saldua BP, Dodge EC, Kolf PR, Olson CA (2018) Reinforced concrete antenna pedestal. Concr Int 40(4):40–42
41. Miller G (2010) Crystal river unit# 3 containment delamination investigation and repair. Progr Energy
42. Dodge EC, Chapa SV (eds) (2015) Impulse response testing-analysis of relative test data. International Symposium on Non-Destructive Testing in Civil Engineering (NDT-CE)
43. Amick H, Xiong B, Tang N, Gendreau M (2009) Voids beneath slabs-on-ground. Concr Int 31(7):29–33